Modelling Structural Deformations in a Roasting Coffee Bean

Nabil T. Fadai[a*], Colin P. Please[b], Robert A. Van Gorder[b]

[a] *School of Mathematical Sciences, Queensland University of Technology, G. P. O. Box 2434, Brisbane, Queensland 4001, Australia*
[b] *Mathematical Institute, University of Oxford, Andrew Wiles Building, Radcliffe Observatory Quarter, Woodstock Road, Oxford OX2 6GG United Kingdom*
[*] *Corresponding author. email: nabil.fadai@qut.edu.au*

Abstract

Macroscale deformations in a roasting coffee bean are important mechanisms in determining flavour development, moisture loss, and consistency of the bean. In this paper, we model the stresses and strains in the cellulose structure of a roasting coffee bean via temperature-dependent poroviscoelastic constitutive equations. This model accounts for the deformations that are created and controlled by the moisture content, temperature, and gas pressure inside of the roasting coffee bean. The model combines previously derived multiphase heat and mass transfer models for roasting coffee beans with these poroviscoeleastic equations, to determine when and where macroscale deformations of the cellular matrix are likely to occur. By exploiting reasonable asymptotic reductions of the poroviscoelastic equations, we find that a large surge of stress is produced in the interior of a coffee bean. We determine that this build-up of stress is due to the viscoelastic interior of the bean being contained by a rigid elastic exterior and unable to expand. Our theoretical results suggest directions for possible improvement in standard industrial coffee roasting techniques, which may allow the macroscale deformations of the cellular matrix to be controlled and thereby improve properties such as flavour, moisture loss, and consistency of the final product.

Keywords: coffee, roasting, first crack, glass transition, poroviscoelasticity

1. Introduction

The coffee industry is valued at more than $100 billion [27] and relies on fundamental research and development to improve the quality and flavour of its product. While simple empirical models and regression analyses have been extensively studied (cf. [1, 26]), mathematical modelling of the coffee roasting process has been largely unexplored. Some notable exceptions include [5], where the authors model the coffee bean in various realistic geometries as a bulk material, and [6, 7, 8], where the authors focus on the phase changes, gas transport, and various chemical reactions in a multiphase setting. While the authors in [6] have addressed the incorporation of multiphase heat and mass transfer and chemical reaction groups into a model describing the roasting of a single coffee bean, the concepts of solid mechanics and structural degradation of the cell walls within a coffee bean during roasting are largely ignored. Incorporating these elements into such models should provide additional insight into macroscopic phenomena that are observed during the roasting process. While the focus of this paper will be on macroscopic deformations in a roasting coffee bean, it is important to note that this phenomena is seen in a variety of applications, including the thermal cracking of baking carbon paste [24], wood drying [20], and popcorn popping [14].

The industrial roasting process of coffee beans is descibed in detail in [1, 7, 26]; we give a brief summary of the key processes. Following the initial drying phase of a coffee roast, which is generally the longest phase of the roast and lasts about 3–6 minutes [1], a phase occurs where flavour and colour start to develop in the bean [1, 26]. This flavour development phase is where the majority of chemical reactions, such as Maillard and pyrolysis reactions, can begin [1, 4, 10, 19, 26]. These reactions generate the colour, flavour, and aromas that are typical of roasted coffee beans [1, 26]. Additionally, carbon dioxide and water vapour is produced within the bean [26]. At some critical point in this stage, one can observe "First Crack" [13], where a distinct popping sound can be heard, not unlike the sound of popping popcorn [13, 26]. After First Crack, the bean's colour continues to darken, while its aromas continue to be enhanced [13, 26]. While a detailed physical explanation for First Crack has not yet been found, it has been hypothesised that First Crack is linked to macro-scale fracturing and deformations of the cellulose structure in a roasting coffee bean.

In this paper, we aim to provide mathematical and physical insight into the causes of First Crack. Specifically, by including solid mechanics effects into our roasting model, we aim to account for macroscopic deformations of the cellulose structure of the coffee bean. We will investigate the structural properties of a coffee bean as it is roasted. In particular, we shall investigate the stresses and strains produced in a coffee bean due to high gas pressures and increasing temperature.

We begin by modelling the cellulose structure of a bean as a poroviscoelastic material. Many similar organic materials, such as wood and fabrics [17, 25], have been modelled in a similar fashion. However, is it generally assumed in these models that the mechanical properties of the material, such as its Lamé coeffficients and viscosities, are constant. It is well known from experimental data (cf. [22, 25]) that these mechanical prop-

erties are strong functions of temperature and change dramatically at a specific *glass transition temperature* [25]. Therefore, we derive the governing poroviscoelastic equations that describe a temperature-dependent poroviscoelastic material in Section 2. Upon non-dimensionalising this model in Section 3, we determine that a dimensionless grouping, usually referred to as the Weissenberg number [23], is large for typical parameter values. By using asymptotic analysis, we determine the leading-order qualitative behaviour of the cellulose structure for the large Weissenberg number limit (discussed in Section 4). These approximations are then compared with numerical results of the full model in Section 5, where additional spherically symmetric geometries of a roasting coffee bean are also considered. A discussion concludes the paper in Section 6.

2. Modelling the Cellulose Structure

In this section, we model the cellulose structure of a roasting coffee bean as a temperature-dependent poroviscoelastic material. Certain simplifications are made to reduce the parameter regime of the poroviscoelastic equations while still being physically reasonable. Additionally, we propose models to describe these temperature-dependent parameters while employing typical values where known. These equations are then further examined in a spherically symmetric domain, where they are in turn coupled to the multiphase models discussed in [6, 7].

2.1. Governing Poroviscoelastic Equations

In order to model deformations within a coffee bean, we must first understand how the solid phase, specifically the cellulose structure, behaves. We begin by assuming that the cellulose material can be represented as an isotropic poroviscoelastic material with a gas pressure, denoted as P, inside the porous structure. Additionally, we assume that only small displacements occur, implying that linear elasticity and viscoelasticity constitutive equations are valid. These assumptions are plausible, as large deformations are not observed until the bean fractures, after which our model will become invalid. Since we anticipate permanent deformations to occur in the bean, we will assume that the elastic and viscous strains of the cellulose are in series (i.e. a Maxwell viscoelastic model [16]). With these assumptions, our constitutive equations for the elastic strain, $\boldsymbol{\epsilon}^e$, and viscous strain, $\boldsymbol{\epsilon}^v$, are related to the effective material stress, $\boldsymbol{\tau}^E$ (given in [16]), by

$$\boldsymbol{\epsilon} = \boldsymbol{\epsilon}^e + \boldsymbol{\epsilon}^v, \tag{1}$$

$$\boldsymbol{\tau}^E = \Lambda(\operatorname{tr}\boldsymbol{\epsilon}^e)\boldsymbol{I} + 2\mathcal{M}\boldsymbol{\epsilon}^e, \tag{2}$$

$$\boldsymbol{\tau}^E = \xi\frac{\partial}{\partial t}(\operatorname{tr}\boldsymbol{\epsilon}^v)\boldsymbol{I} + 2\eta\frac{\partial \boldsymbol{\epsilon}^v}{\partial t}. \tag{3}$$

Here, Λ and $\mathcal{M}$ are the Lamé coefficients of the cellulose material, while ξ and η are the bulk and shear viscosities of the cellulose, respectively [16]. We then combine the constitutive equations (1)–(3) to obtain

$$\frac{\partial}{\partial t}\left[\frac{\boldsymbol{\tau}^E}{\Lambda}\right] + \frac{\boldsymbol{\tau}^E}{\xi} = \frac{\partial}{\partial t}\left[(\operatorname{tr}\boldsymbol{\epsilon})\boldsymbol{I} + 2\frac{\eta}{\xi}\boldsymbol{\epsilon} + 2\left(\frac{\mathcal{M}}{\Lambda} - \frac{\eta}{\xi}\right)\boldsymbol{\epsilon}^e\right] - 2\boldsymbol{\epsilon}\frac{\partial}{\partial t}\left[\frac{\eta}{\xi}\right]. \tag{4}$$

Finally, we decompose the total stress, $\boldsymbol{\tau}$, using Terzaghi's stress principle (see, e.g., [28]) as the difference of the effective stress of the cellulose and the total gas pressure, P, in the material: $\boldsymbol{\tau} = \boldsymbol{\tau}^E - P\boldsymbol{I}$. This is coupled with the steady-state conservation of linear momentum equation, as we assume that the acceleration of the displacement of cellulose is negligible:

$$\boldsymbol{\nabla}\cdot\boldsymbol{\tau} = \boldsymbol{0}. \tag{5}$$

2.2. Reducing the Parameter Regime

While the Lamé coefficients and viscosities of the cellulose matrix are all functions of temperature, we will now make standard assumptions concerning viscoelastic materials to reduce the degrees of freedom in the model. Specifically, we assume that the ratio of viscosities is equal to the ratio of Lamé parameters, i.e.

$$\frac{\mathcal{M}}{\Lambda} = \frac{\eta}{\xi} := \frac{2-\varsigma}{2\varsigma}. \tag{6}$$

This simplification is often taken with viscoelastic materials (c.f. [16]) and is equivalent to stating that the elastic and viscous components have the same Poisson's ratio, $\nu = \varsigma/(\varsigma+2)$. Additionally, we will assume that the ratio $\frac{\mathcal{M}}{\Lambda}$ is constant (i.e., that ς is constant). In consequence, (4) reduces to

$$\frac{\partial}{\partial t}\left[\frac{\boldsymbol{\tau}^E}{\Lambda}\right] + \frac{\boldsymbol{\tau}^E}{\xi} = \frac{\partial}{\partial t}\left[(\operatorname{tr}\boldsymbol{\epsilon})\boldsymbol{I} + \left(\frac{2-\varsigma}{\varsigma}\right)\boldsymbol{\epsilon}\right]. \tag{7}$$

2.3. The Glass Transition Temperature

Along with the aforementioned assumptions concerning the Lamé coefficients and viscosities of the cellulose matrix, we also anticipate that the cellulose structure in a coffee bean will significantly change material properties at its *glass transition temperature* [25]. Specifically, the glass transition temperature represents the transition in amorphous materials from behaving like a brittle (or, elastic) material to a rubbery (or, viscous) material. Crucially, this glass transition temperature, denoted here as T_G, also depends on the material's moisture content [25]. A simple empirical relationship for T_G, which agrees with qualitative features seen in experimental data, is given by

$$T_G(Y) = T_{\text{dry}}\left[1 + \frac{Y}{Y^*}\left(\frac{T_{\text{dry}}}{T_0} - 1\right)\right]^{-1}, \tag{8}$$

where Y is the mass fraction of water, T_{dry} is the glass transition temperature at zero moisture, and Y^* is the mass fraction at which the glass transition occurs at room temperature (T_0). The quantity Y is related to the water saturation by

$$Y = \left[1 + \frac{\rho_s(1-\phi)}{\rho_w\phi S}\right]^{-1}, \tag{9}$$

where ϕ is the porosity of the coffee bean, S is the water saturation, and ρ_s, ρ_w are the densities of cellulose and water, respectively. This puts (8) into the form

$$T_G(\phi, S) = \frac{T_{\text{dry}}\left(1 + \frac{\rho_s(1-\phi)}{\rho_w\phi S}\right)}{1 + \frac{\rho_s(1-\phi)}{\rho_w\phi S} + \frac{1}{Y^*}\left(\frac{T_{\text{dry}}}{T_0} - 1\right)}. \tag{10}$$

When the temperature locally within the bean is below the glass transition temperature, we expect that the cellulose behaves elastically; that is to say, the viscosity of the cellulose is very large in comparison to the elasticity parameters. Above the glass transition temperature, however, the cellulose will permanently deform due to viscous effects. This implies that, unlike previously described poroviscoelastic models (c.f. [16]), the viscosities and/or the Lamé coefficients of the cellulose will vary with temperature. The authors of [22] observed that these parameters in coffee beans decrease in a sigmoidal manner near the glass transition temperature. Similar sigmoidal behaviour has also been observed in other materials' mechanical properties as a function of temperature (c.f. [11, 15]). While there are a variety of constitutive equations that can be employed, we propose a simple model to reflect this sigmoidal behaviour in Λ and ξ observed in experiments:

$$\Lambda = \frac{\lambda_1 + \lambda_2}{2} + \left(\frac{\lambda_2 - \lambda_1}{2}\right)\tanh\left(\frac{T - T_G(\phi, S)}{T_{\text{crit}}}\right), \tag{11}$$

$$\xi = \frac{\xi_1 + \xi_2}{2} - \left(\frac{\xi_1 - \xi_2}{2}\right)\tanh\left(\frac{T - T_G(\phi, S)}{T_{\text{crit}}}\right). \tag{12}$$

Here, λ_1 and λ_2 are the Lamé coefficients of the cellulose at low and high temperatures, ξ_1 and ξ_2 are the viscosities of the cellulose at low and high temperatures, and we define T_{crit} as a physical parameter representing the sharpness of the sigmoidal transition. A small value of T_{crit} represents a sharp and rapid transition between parameter regimes, whereas a larger value of T_{crit} represents a more gradual change in the cellulose's elastic and viscous properties. As we anticipate a larger viscosity and/or Lamé coefficient when $T < T_G$, we will assume that $\lambda_1 > \lambda_2$ and $\xi_1 > \xi_2$.

Naturally, there are many other forms of Λ and ξ that could be chosen to represent the sigmoidal behaviour observed in experiments near the glass transition. However, the authors in [22] note that the temperature range in which significant changes to the Lamé coefficients and viscosities occur is small, relative to the total temperature range across an entire roast. Therefore, any changes to the proposed function form of (11) and (12) will only marginally affect the behaviour of the cellulose material near the glass transition temperature.

2.4. Parameter Values Associated with the Glass Transition Temperature

It is expected that, in an isothermal setting, the Lamé coefficient λ_1 will be a function of porosity and water saturation, which reflects the porous cellulose structure. Using the isothermal closed cell model proposed in [12], which is a suitable model to describe the porous structure of a coffee bean, we infer the empirical relationship

$$\frac{\lambda_1}{\Lambda^*} \sim \phi^2\left(1 - \phi + \phi S\frac{\rho_w}{\rho_s}\right)^2 + (1 - \phi)\left(1 - \phi + \phi S\frac{\rho_w}{\rho_s}\right). \tag{13}$$

Here, Λ^* represents the Lamé coefficient of solid cellulose ($\approx$ 59600 atm, [29]) and $\frac{\rho_w}{\rho_s}$ is the density ratio of water to solid cellulose ($\approx$ 1.18, [2]). As seen in [6, 7], we anticipate that $\phi \approx 0.5$ and $S \in [0, 0.1]$, which suggests that $\frac{\lambda_1}{\Lambda^*} \in [0.31, 0.36]$. Therefore, we assume that at low temperatures, $\lambda_1 \approx 0.335\Lambda^* \approx 2\times10^4$ atm. Typical values of the Lamé coefficients of cellulose have been examined extensively in [29]; from these values, we assume that $\varsigma \approx 0.72$. It is unclear how large λ_2 should be, however, we shall see later that the choice of λ_2 does not affect the dominant behaviour of the cellulose deformations.

We also find that it is unclear how large ξ_1 should be in order to reflect that the deformations below the glass transition temperature are purely elastic; we use a theoretical upper bound (c.f. [9]) and impose that $\xi_1 \leq 10^{12}$ Pa·s. From measurements of viscosity for various wood/plastic composite materials (c.f. [17]), these indicate that $\xi_2 \approx 10^5$ Pa·s is a reasonable choice to make.

Finally, is it important to determine typical parameter values used in the glass transition temperature (10). These parameter values have been recorded for coffee beans, see e.g. [22], hence we take $T_{\text{crit}} \in [10°\text{C}, 30°\text{C}]$, $T_{\text{dry}} \approx 190°\text{C}$, $Y^* \approx 0.995$.

2.5. Governing Equations under Spherical Symmetry

Having discussed how the Lamé coefficients and viscosities are temperature-dependent, along with their typical parameter values, we now return to the poroviscoelastic equations described in Section 2.1 to model deformations in the cellulose structure and examine the special, but physically relevant case, of spherical symmetry. In a spherically symmetric domain with symmetric boundary conditions, the displacement $\mathbf{u}$ is purely radial (i.e., $\mathbf{u} = [u(r), 0, 0]^\top$, where $^\top$ denotes transposition) and (5) reduces to

$$\tau_{\theta\theta} = \frac{1}{2r}\frac{\partial}{\partial r}\left(r^2\tau_{rr}\right), \tag{14}$$

where τ_{rr} and $\tau_{\theta\theta}$ denote the radial and hoop (angular) stresses, respectively. Additionally, the radial and angular strains, e_{rr} and $e_{\theta\theta}$, can be written as

$$e_{rr} = \frac{\partial u}{\partial r}, \qquad e_{\theta\theta} = \frac{u}{r}, \tag{15}$$

respectively. Therefore, we can determine the radial and angular components of (7), and obtain

$$\frac{\partial}{\partial t}\left[\frac{\tau_{rr} + P}{\Lambda}\right] + \frac{\tau_{rr} + P}{\xi} = \frac{\partial}{\partial t}\left[\frac{1}{r^2}\frac{\partial}{\partial r}(r^2 u) + 2\frac{\eta}{\xi}\frac{\partial u}{\partial r}\right], \tag{16}$$

$$\frac{\partial}{\partial t}\left[\frac{1}{\Lambda}\frac{\partial \tau_{rr}}{\partial r} + \frac{\partial}{\partial r}\left(\frac{4\eta u}{\xi r}\right)\right] + \frac{1}{\xi}\frac{\partial \tau_{rr}}{\partial r} = 0. \tag{17}$$

As we will see in Section 2.6, we have more information at the boundaries of the coffee bean for u than for τ_{rr}. Therefore, we manipulate (16)–(17) to eliminate explicit spatial derivatives in τ_{rr}. Firstly, (16)–(17) can be expressed as

$$\frac{\partial \tau_{rr}}{\partial t} = -\frac{\partial P}{\partial t} + \Lambda\left[\frac{2}{\varsigma}\frac{\partial^2 u}{\partial t \partial r} + \frac{2}{r}\frac{\partial u}{\partial t} - (\tau_{rr} + P)\Omega\right], \tag{18}$$

$$\frac{\partial \tau_{rr}}{\partial r}\Omega = -\frac{1}{\Lambda}\frac{\partial^2 \tau_{rr}}{\partial t \partial r} - \left(\frac{4 - 2\varsigma}{\varsigma}\right)\frac{\partial}{\partial r}\left(\frac{1}{r}\frac{\partial u}{\partial t}\right), \tag{19}$$

where

$$\Omega = \frac{1}{\xi} - \frac{1}{\Lambda^2}\frac{\partial \Lambda}{\partial t}. \tag{20}$$

Substituting (18) into (19) yields, after some rearranging of terms,

$$\begin{aligned}\frac{\partial}{\partial r}\left[\Lambda\left(\frac{2}{\varsigma}\frac{\partial^2 u}{\partial t \partial r} + \frac{2}{r}\frac{\partial u}{\partial t}\right)\right] + \left(\frac{4-2\varsigma}{\varsigma}\right)\frac{\partial}{\partial r}\left(\frac{1}{r}\frac{\partial u}{\partial t}\right) \\ = \frac{\partial^2 P}{\partial t \partial r} + (\tau_{rr} + P)\frac{\partial}{\partial r}(\Lambda\Omega) + \Lambda\Omega\frac{\partial P}{\partial r}.\end{aligned} \tag{21}$$

This then allows us to couple (18) to the following second-order differential equation for the material's velocity $\frac{\partial u}{\partial t}$

$$\begin{aligned}\frac{\partial^3 u}{\partial t \partial r^2} + \frac{\partial u}{\partial t \partial r}\left(\frac{1}{\Lambda}\frac{\partial \Lambda}{\partial r} + \frac{2}{r}\right) + \frac{1}{r}\frac{\partial u}{\partial t}\left(\frac{\varsigma}{\Lambda}\frac{\partial \Lambda}{\partial r} - \frac{2}{r}\right) \\ = \frac{\varsigma}{2\Lambda}\left[\frac{\partial^2 P}{\partial t \partial r} + (\tau_{rr} + P)\frac{\partial}{\partial r}(\Lambda\Omega) + \Lambda\Omega\frac{\partial P}{\partial r}\right].\end{aligned} \tag{22}$$

We will refer to equations (18) and (22) as the poroviscoelastic equations.

2.6. Boundary and Initial Conditions

We assume that the bean starts from a reference state of zero displacement, i.e., a strain-free initial state, giving

$$u = 0 \text{ and } \tau_{rr} = -P \text{ at } t = 0. \tag{23}$$

When modelling a coffee bean as a solid sphere of radius L, we also have that there is zero displacement at the centre of the bean, along with zero radial strain at the surface of the bean; this is equivalent to

$$u = 0 \text{ at } r = 0 \quad \text{and} \quad \frac{\partial u}{\partial r} = 0 \text{ at } r = L. \tag{24a}$$

However, as was discussed in [6], a more accurate representation of a coffee bean in a spherically symmetric geometry could be a spherical "shell" of outer radius L and inner radius aL. This is to aid in preserving not only the volume of the coffee bean, but also the average square-distance from any point in the bean to the boundary. In the geometry, we impose zero radial strain at both the inner and outer surfaces of the bean:

$$\frac{\partial u}{\partial r} = 0 \text{ at } r = aL \quad \text{and} \quad \frac{\partial u}{\partial r} = 0 \text{ at } r = L. \tag{24b}$$

2.7. Determining the Gas Pressure

In order to determine the deformations that occur from the increasing gas pressure inside the bean, we must also determine the pressure, P, from other conservation equations. While we can use more complicated models that account for chemical reactions and additional gas species, such as the Sugar Pathway Model in [7], we will focus on a simpler (and better understood) model to highlight the effects of solid mechanics. In particular, we use a multiphase model motivated from [8] to highlight moisture and vapour transport in a roasting coffee bean. However, the multiphase model used in [8] should also incorporate a *sorption isotherm* to account for various evaporation mechanisms present a roasting coffee bean, as was done in [6]. This can be done by changing the steam table pressure for pure water, denoted as $P_{ST}(T)$ in [8], to the sorption isotherm from [6]:

$$P_v^*(T, S) = \frac{S^{C_1}\exp\left(D_1 P_0 \frac{D_2 T_0 (T - T_\infty)}{(T_\infty - T_0)T}\right)}{S^{C_1} + C_2 \sigma^{C_1}}. \tag{25}$$

Here, D_1 and D_2 are the steam table values for pure water [3], C_1 and C_2 are water activity parameters used in the Oswin sorption isotherm (discussed in detail in [6, 21]), T_∞ is the temperature of the coffee roaster, T_0 is room temperature, σ is the initial saturation of the bean, and P_0 is atmospheric pressure.

As we do not expect large deformations to occur in the bean before First Crack, we can neglect any advection caused by the moving cellulose. Consequently, this implies that this multiphase model from [8] decouples from the poroviscoelastic equations described previously. We can therefore solve the multiphase model in a fixed geometry to determine T, S, and P before determining τ_{rr} and u via the poroviscoelastic equations. Finally, to observe a significant build-up of vapour pressure, we assign the gas permeability to be $k_g = 10^{-16}$ m^2, which agrees with typical parameter values discussed in [6].

3. The Non-dimensionalised Poroviscoelastic Equations and Multiphase Model

In order to better understand the governing conservation equations (18) and (22), we non-dimensionalise the system variables according to $P = \mathcal{P}\hat{P}$, $T = T_0 + (T_\infty - T_0)\hat{T} := T_0(1 + \mathscr{T}\hat{T})$, $\tau_{rr} = \mathcal{P}\hat{\tau}$, $\Lambda = \frac{\lambda_1}{2}\hat{\Lambda}$, $\xi = \frac{\xi_2}{2}\hat{\xi}$, $\Omega = \frac{2}{\xi_2}\hat{\Omega}$, $S = \sigma\hat{S}$, $r = L\hat{r}$, $t = \vartheta\hat{t}$, $u = \frac{L\mathcal{P}\vartheta}{\xi_2}\hat{u}$. Here, the typical pressure, $\mathcal{P}$, and vapour diffusive timescale, ϑ, are identical to the values used in the non-dimensionalisation in [8], i.e. $\mathcal{P} = D_1 P_0$ and $\vartheta = \frac{\phi\mu L^2}{k_{g0}\mathcal{P}}$. Using these scalings in the poroviscoelastic equations (18) and (22) gives

$$\frac{\partial \tau_{rr}}{\partial t} = -\frac{\partial P}{\partial t} + \mathrm{Wi}\,\Lambda\left[\frac{1}{\varsigma}\frac{\partial^2 u}{\partial t \partial r} + \frac{1}{r}\frac{\partial u}{\partial t} - (\tau_{rr} + P)\Omega\right], \tag{26}$$

$$\begin{aligned}\frac{\partial^3 u}{\partial t \partial r^2} + \frac{\partial u}{\partial t \partial r}\left(\frac{1}{\Lambda}\frac{\partial \Lambda}{\partial r} + \frac{2}{r}\right) + \frac{1}{r}\frac{\partial u}{\partial t}\left(\frac{\varsigma}{\Lambda}\frac{\partial \Lambda}{\partial r} - \frac{2}{r}\right) \\ = \frac{\varsigma}{\Lambda}\left[\frac{1}{\mathrm{Wi}}\frac{\partial^2 P}{\partial t \partial r} + (\tau_{rr} + P)\frac{\partial}{\partial r}(\Lambda\Omega) + \Lambda\Omega\frac{\partial P}{\partial r}\right],\end{aligned} \tag{27}$$

where the relevant dimensionless functions are defined as

$$\Omega = \frac{1}{\xi} - \frac{1}{\mathrm{Wi}\,\Lambda^2}\frac{\partial \Lambda}{\partial t}, \tag{28}$$

$$\Lambda = 2 - \varphi_1\left[1 + \tanh\left(\frac{1 + \mathscr{T}T - T_G}{\varphi_3}\right)\right], \tag{29}$$

$$\xi = 2 + \varphi_2\left[1 - \tanh\left(\frac{1 + \mathscr{T}T - T_G}{\varphi_3}\right)\right], \tag{30}$$

$$T_G(S) = \frac{\frac{T_{\mathrm{dry}}}{T_0}\left(S + \frac{\rho_s(1-\phi)}{\rho_w \phi \sigma}\right)}{\frac{\rho_s(1-\phi)}{\rho_w \phi \sigma} + \frac{S}{Y^*}\left(\frac{T_{\mathrm{dry}}}{T_0} - 1 + Y^*\right)}. \tag{31}$$

We have introduced the new dimensionless groups $\mathrm{Wi} = \frac{\lambda_1 \vartheta}{\xi_2}$, $\varphi_1 = 1 - \frac{\lambda_2}{\lambda_1}$, $\varphi_2 = \frac{\xi_1}{\xi_2} - 1$, and $\varphi_3 = \frac{T_{\mathrm{crit}}}{T_0}$. The dimensionless parameter Wi is often referred to as the *Weissenberg number* [23], which relates the elastic strains in the cellulose to the viscous strains. Additionally, the dimensionless parameters φ_1 and φ_2 determine the relative changes in the Lamé coefficients and viscosities at the glass transition temperature, whereas φ_3 indicates how sharp the transition is. While the Lamé coefficients have been observed in experiments to be temperature-dependent, the coefficients do not change usually by more than one order of magnitude. Therefore, we will focus our subsequent analysis in Section 4 to the assumption that $\varphi_1 = O(1)$ or smaller. However, the authors in [22] note significant changes in viscosities over a roast, which is linked to the magnitude of the dimensionless grouping φ_2. Therefore, our analysis in Section 4 assumes that φ_2 is large. Finally, in order to match experimental data seen in [22], we will assume that the transition in viscosities occurs in a small temperature range near the glass transition temperature (i.e. that φ_3 is small).

To determine how the temperature in a coffee bean changes throughout the roast, we use the multiphase models described in [6, 7, 8], which we couple to the poroviscoelastic equations (26)–(27). These multiphase models focus on the local moisture activity and use parameter values specifically chosen to agree with experimental data for roasting coffee beans. This, in turn, allows us to couple the water saturation, vapour pressure, and temperature to the mechanical properties of the cellulose structure. The model reads

$$\frac{\partial S}{\partial t} = -\frac{1}{\epsilon^2} I_v, \tag{32}$$

$$\frac{\partial}{\partial t}\left[\frac{(1+\mathscr{T})P(1-\sigma S)}{1+\mathscr{T}T}\right] = -\frac{1}{\delta}\frac{\partial S}{\partial t} + \nabla\cdot\left[\frac{(1+\mathscr{T})P\nabla P}{1+\mathscr{T}T}\right], \tag{33}$$

$$\frac{\partial T}{\partial t} + \mathcal{A}_1\frac{\partial}{\partial t}\left[S(1+\mathscr{T}T)\right] = \mathcal{A}_2\frac{\partial S}{\partial t} + \mathcal{A}_3\nabla\cdot\left[(1+\mathcal{A}_4 S)\nabla T\right], \tag{34}$$

where

$$I_v = S(1-\sigma S)(P_v^*(T,S) - P)\sqrt{\frac{1+\mathscr{T}}{1+\mathscr{T}T}} \tag{35}$$

and

$$P_v^*(T,S) = \frac{S^{C_1}\exp\left(\frac{D_2(T-1)}{1+\mathscr{T}T}\right)}{S^{C_1}+C_2}. \tag{36}$$

Following [6, 7, 8], we note that ϵ represents the timescale ratio between evaporation and vapour diffusion, whereas δ represents the density ratio between water vapour and water. Furthermore, $\mathcal{A}_1$, $\mathcal{A}_3$, and $\mathcal{A}_4$ represent effective thermal properties of the roasting bean in a multiphase setting, whereas $\mathcal{A}_2$ is related to the latent heat of evaporation. The evaporation rate I_v is based on Langmuir's equation [18], but includes the sorption isotherm P_v^*, which in non-dimensional quantities is given in (36). Typical parameter values used are listed in Table 1.

In the solid sphere geometry, our boundary conditions become

$$u = 0, \quad \frac{\partial T}{\partial r} = 0, \quad \frac{\partial P}{\partial r} = 0 \ \text{ at } \ r = 0, \tag{37}$$

Dimensionless Group	Typical value of Parameter
ϵ	1.40×10^{-4}
δ	0.101
σ	0.10
$\mathcal{A}_1$	1.50
$\mathcal{A}_2$	2.81
$\mathcal{A}_3$	2.28
$\mathcal{A}_4$	0.899
C_1	0.41
C_2	6.1×10^{-3}
D_1	35.0
D_2	7.31
Nu	0.585
P_a	0.0879

Table 1: Typical values of dimensionless parameters used in the multiphase model. Parameter values are obtained from dimensional quantities listed in [6, 7, 8].

$$\frac{\partial T}{\partial r} = \mathrm{Nu}\left(\frac{1-\sigma S}{1-\sigma}\right)\left(\frac{1+\mathcal{A}_4}{1+\mathcal{A}_4 S}\right)(1-T) \ \text{ at } \ r = 1, \tag{38}$$

$$P = \begin{cases} P_v^*(T,S), & T < T_a, \\ P_a, & T \geq T_a, \end{cases} \ \text{ at } \ r = 1, \tag{39}$$

$$\frac{\partial u}{\partial r} = 0 \ \text{ at } \ r = 1. \tag{40}$$

If we use the spherical shell geometry instead, our boundary conditions become

$$\frac{\partial T}{\partial r} = \mathrm{Nu}\left(\frac{1-\sigma S}{1-\sigma}\right)\left(\frac{1+\mathcal{A}_4}{1+\mathcal{A}_4 S}\right)(1-T) \ \text{ at } \ r = a, 1, \tag{41}$$

$$P = \begin{cases} P_v^*(T,S), & T < T_a, \\ P_a, & T \geq T_a, \end{cases} \ \text{ at } \ r = a, 1, \tag{42}$$

$$\frac{\partial u}{\partial r} = 0 \ \text{ at } \ r = a, 1. \tag{43}$$

Finally, our initial conditions in both geometries are

$$\begin{aligned} S(r,0) = 1, \ \ T(r,0) = 0, \ \ P(r,0) = P_v^*(0,1), \\ u(r,0) = 0, \ \ \text{and} \ \ \tau_{rr}(r,0) = -P(r,0). \end{aligned} \tag{44}$$

4. The Large Wi and φ_2 Limit

Typical parameter values (as derived in Section 2.4) indicate that $\mathrm{Wi} \approx 5.5\times10^3$, so it is natural to perform an asymptotic analysis in the large Weissenberg number limit. However, in the case where all other parameters are $O(1)$, our analysis suggests that the leading-order displacement u_0 will be $O(1)$, which yields a dimensional displacement of $\frac{L\mathcal{P}\vartheta}{\xi_2} \approx 40$mm after roasting, which is clearly too large for a coffee bean. One way of addressing this nonphysical result is to modify the displacement by considering a large value of φ_2 in the poroviscoelastic equations. Indeed, the case where φ_2 is large is more physically relevant to coffee bean roasting due to anticipated large changes in viscosity.

We assume $\varphi_2 = \mathrm{Wi}^\alpha$ for $\alpha > 0$. There is a distinguished limit when $\alpha = 1$, which divides the parameter regime into two main regions: $0 < \alpha < 1$ and $\alpha > 1$. As we do not know ξ_1, it is possible that any of these three regimes may be physically relevant. We take the asymptotic expansions in the limit $\mathrm{Wi}^{-\alpha} \to 0$ to be

$$u(r,t) = \mathrm{Wi}^{-\alpha} U_0(r,t) + O(\mathrm{Wi}^{-2\alpha}), \quad \tau_{rr}(r,t) = \mathcal{T}_0(r,t) + O(\mathrm{Wi}^{-\alpha}). \tag{45}$$

The regime $0 < \alpha < 1$ corresponds to the viscous strains being small below the glass transition temperature, which in turn implies that $u \ll 1$ when $1 + \mathscr{T}T < T_G$. The leading order equations from (26) and (27) resulting from the expansion (45) may then be reduced to a single partial differential equation for U_0,

$$\frac{\partial^3 U_0}{\partial t \partial r^2} + \frac{\partial U_0}{\partial t \partial r}\left(\frac{1}{\Xi}\frac{\partial \Xi}{\partial r} + \frac{2}{r}\right) + \frac{1}{r}\frac{\partial U_0}{\partial t}\left(\frac{\varsigma}{\Xi}\frac{\partial \Xi}{\partial r} - \frac{2}{r}\right) = \frac{\varsigma}{\Xi}\frac{\partial P}{\partial r}, \tag{46}$$

where the rescaled viscosity Ξ is defined as

$$\Xi = 1 - \tanh\left(\frac{1 + \mathscr{T}T - T_G}{\varphi_3}\right). \tag{47}$$

Subject to appropriate boundary conditions, a solution U_0 from (46) remains $O(1)$ when $1 + \mathscr{T}T < T_G$, provided that the time integral of the pressure gradient remains $O(1)$. We conclude that for $0 < \alpha < 1$, the displacement u is $O(\mathrm{Wi}^{-\alpha})$ at leading order, and hence the displacement will now scale as $40\mathrm{Wi}^{-\alpha}$mm. As $\mathrm{Wi} \approx 5.5 \times 10^3$, this suggests the range $0.35 < \alpha < 0.6$ is appropriate in order to obtain physically reasonable displacements of size 0.2mm to 2mm. We shall later demonstrate displacements within this range when discussing numerical experiments in Section 5, suggesting that this is the appropriate regime for α.

The distinguished limit $\alpha = 1$ corresponds to the inclusion of temporal stress terms in (26) and (27) in the leading-order equations. Therefore, $\varphi_2 = C\mathrm{Wi}$ and $C = O(1)$. The leading order equations while $1 + \mathscr{T}T < T_G$ are not great simplifications of (26) and (27), so we omit them. The main conclusion from this distinguished limit regime is that deformations taking place while $1 + \mathscr{T}T < T_G$ are negligible in comparison to the $O(1)$ deformations that occur when $1 + \mathscr{T}T > T_G$ (i.e., $\xi \sim 2$). Indeed, since deflections scale as $40\mathrm{Wi}^{-\alpha}$mm, $\alpha = 1$ implies negligible deflections of size 0.007mm, roughly 500 times less than the radius of the bean. Similarly, for the case of $\alpha > 1$, any resulting deflections will be negligibly small for $1 + \mathscr{T}T < T_G$, in comparison to the $O(1)$ deformations that occur when $1 + \mathscr{T}T > T_G$.

5. Numerical Simulations and Results

We solve the poroviscoelastic equations (26)–(27), coupled with the multiphase model (32)–(44), in both aforementioned spherically symmetric geometries in MATLAB, using a second-order finite difference scheme in the spatial component and a stiff ODE solver for the time component (namely, the MATLAB function `ode23s`). We used 101 spatial meshpoints to achieve good numerical resolution.

We first examine the solid sphere geometry (of radius $r = 4$mm) in order to explore the effects of a temperature-dependent viscosity. Numerical difficulties are observed for sharp sigmoidal behaviour in viscosities, e.g., values of φ_3 smaller than 0.04, corresponding to $T_{\mathrm{crit}} < 10°\mathrm{C}$. In order to avoid these numerical difficulties, we relax this sharp transition and take $\varphi_3 \approx 0.09$, corresponding to $T_{\mathrm{crit}} = 25°\mathrm{C}$. We plot displacements for two distinct values of φ_2 in Figure 1, finding that the displacements are smaller when the temperature is below the glass transition temperature than in the constant viscosity parameter regime (Figure 2(a)). Furthermore, as seen in Figures 2(b)–(c), the leading-order solution for displacement, U_0, determined via equation (46), accurately matches the displacement profile for φ_1 non-zero with less than a 3% relative error. However, as seen in Figure 3(a), a large spike in radial stress takes place when the surface of the bean reaches the glass transition temperature. This spike in stress is caused by a thin region near the coffee bean's surface becoming far more rigid that its viscous interior. Mechanical failure in the solid structure, resulting in First Crack, may therefore be linked to this spike in stress. Once the glass transition has occurred at the surface of the bean, and if the surface does not fail, the viscosity of the cellulose dissipates the build-up of stress.

We next compare the model solutions for a solid sphere geometry with those obtained for a spherical shell geometry. As the geometry changes, certain non-dimensional grouping will also change in value. For example, going from a solid sphere of radius 4mm to a spherical shell of outer radius 3.28mm and inner radius 1.54mm [6], the Weissenberg number changes from $\mathrm{Wi} \approx 5.5 \times 10^3$ to $\mathrm{Wi} \approx 3.7 \times 10^3$. In Figure 3, the resulting change in stress between these two geometries is shown. In particular, in Figure 3(b), we observe that the glass transition temperature is attained first in the interior of the bean, but then propagates outward toward both surfaces of the bean. This produces a spike of radial stress that persists until the glass transition temperature is attained at both the inner and outer radii. While the spherical shell geometry captures more of the realistic features of a roasting coffee bean, most of the qualitative features are observed for the solid sphere geometry.

Our results suggest that macro-scale fracturing of a roasting coffee bean can be controlled by manipulating when the glass transition temperature is first attained at the surface of the bean. One possibility is to modify the convective heat coefficient at the surface of the bean (contained in the non-dimensional grouping Nu), so that the effective thermal timescale of the problem is changed. Alternatively, the roasting temperature could be changed (contained in the non-dimensional grouping $\mathscr{T}$) so that the glass transition temperature occurs at a different moisture value. In either case, altering the roasting environment of the bean will modify when the glass transition temperature is attained at various positions within the bean, hence changing the time at which First Crack occurs.

6. Discussion

Motivated by the phenomenon of "First Crack", we have developed a model for the stresses and strains in the cellu-

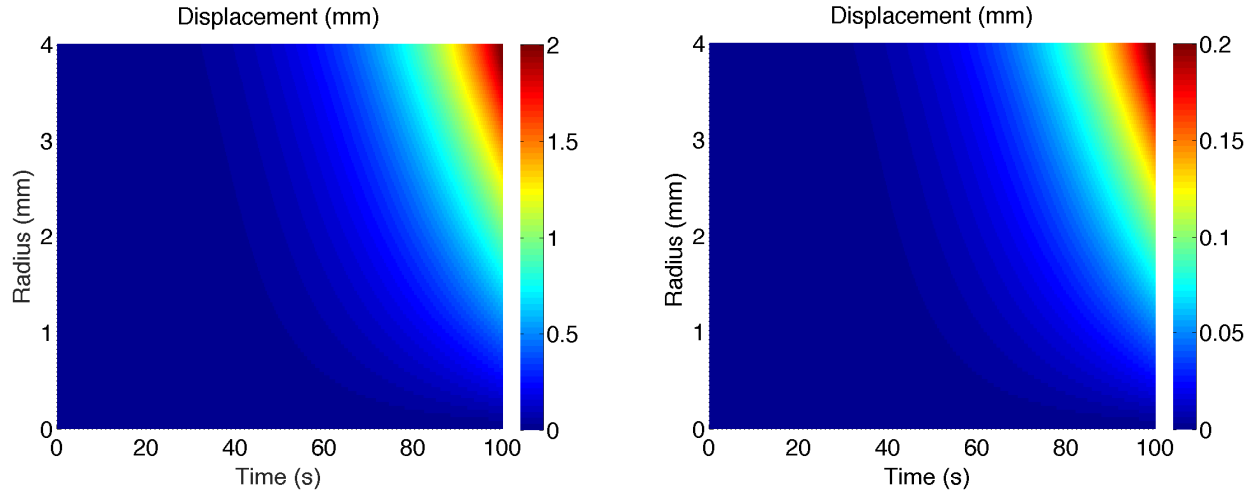

(a) (b)

Figure 1: The radial displacement $u(r,t)$ of the poroviscoelastic equations in the solid sphere geometry, with $\varphi_1 = 0$, $\varphi_3 = 0.09$ and temperature-dependent viscosity ξ, with (a) $\varphi_2 = 9$ and (b) $\varphi_2 = 99$. As φ_2 increases, the radial displacement at a given location decreases in magnitude (as seen in the color bar for each panel), which is in agreement with the findings of Section 4. However, note that the overall distribution of displacements remains very much the same between the two panels.

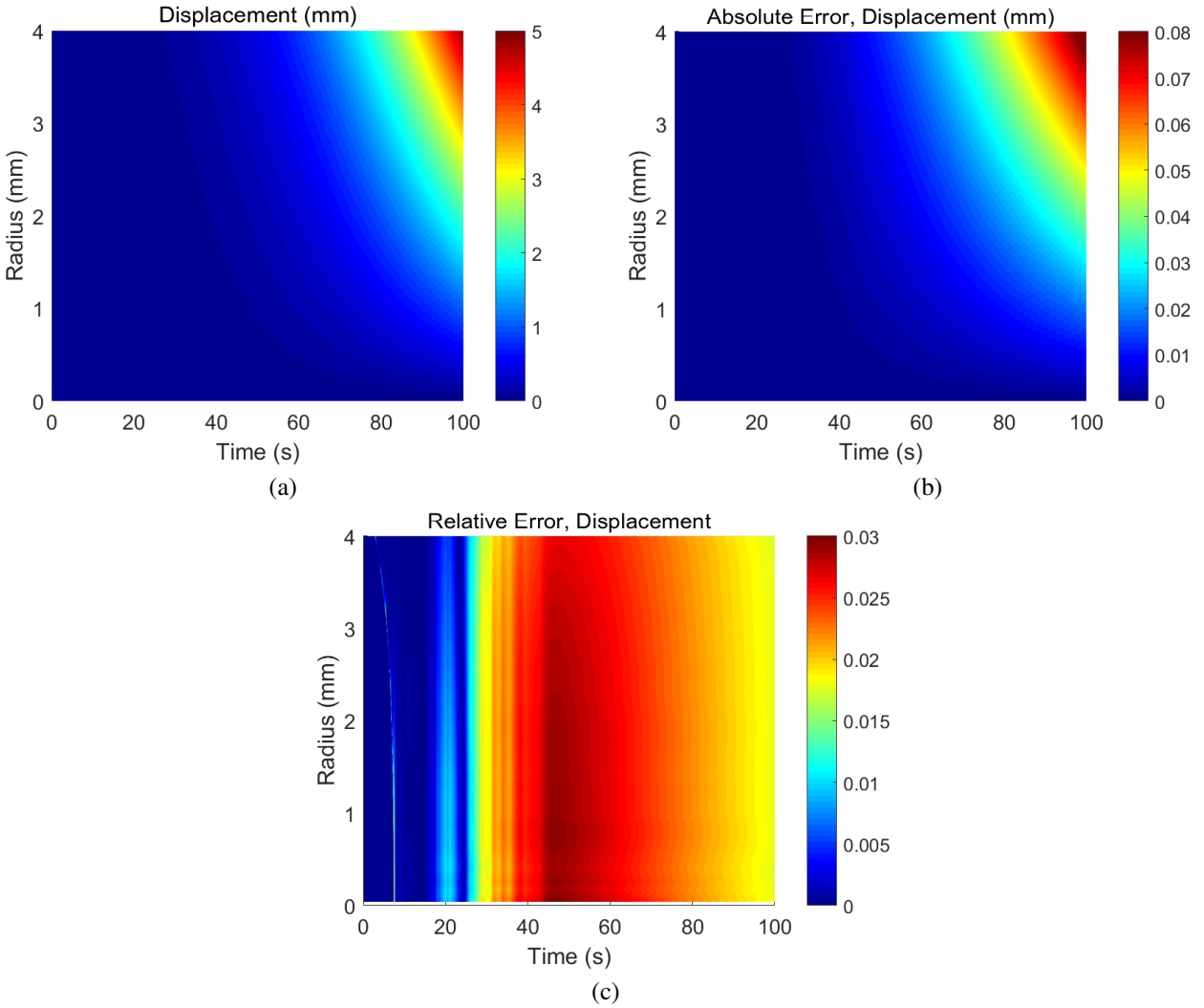

(a) (b)

(c)

Figure 2: (a) The radial displacement $u(r,t)$ of the poroviscoelastic equations in solid sphere geometry, with a temperature-dependent Lamé coefficient ($\varphi_1 = 0.25$, $\varphi_2 = 0$, $\varphi_3 = 0.09$). (b) The absolute error $|u(r,t) - U_0(r,t)|$ and (c) the relative error $|u(r,t) - U_0(r,t)|/u(r,t)$, where $U_0(r,t)$ is the leading-order approximation in the large Weissenberg number limit determined via equation (46).

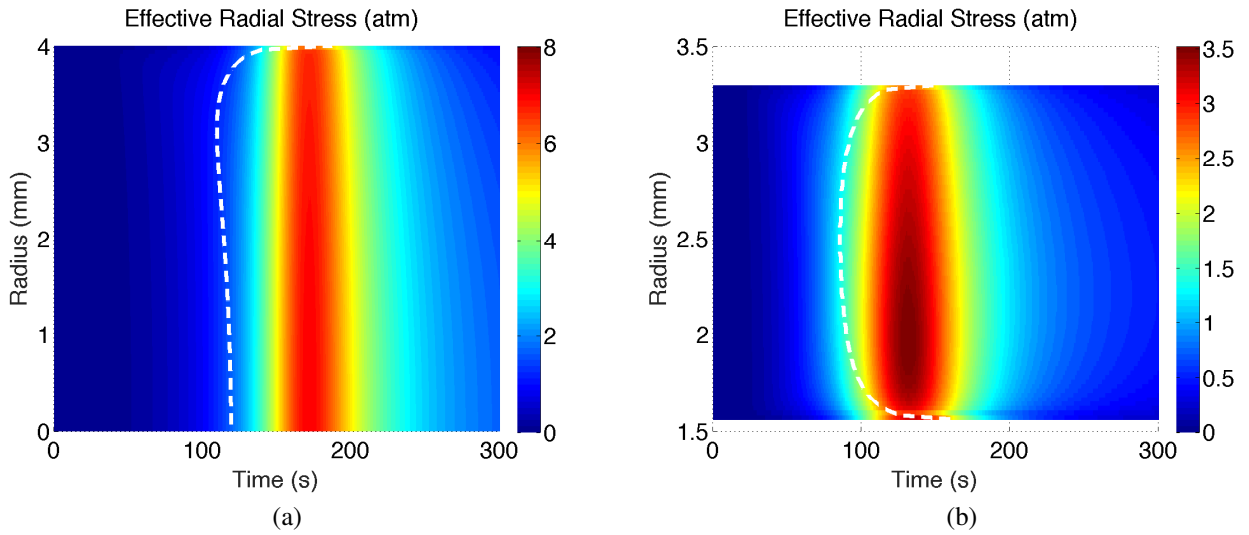

Figure 3: The effective radial material stress $\tau^E_{rr}(r,t)$ of the poroviscoelastic equations, with $\varphi_1 = 0$, $\varphi_2 = 9$, and $\varphi_3 = 0.09$, in (a) solid sphere geometry and (b) spherical shell geometry. A large build-up of stress is observed when the glass transition temperature (white dashed curves) approaches the surface(s) of the bean.

lose structure of a roasting coffee bean. As First Crack occurs roughly at the same time as many flavour development chemical reactions, understanding First Crack from a more theoretical standpoint is important for determining other key features of the roasting process. We first modelled the cellulose structure in the bean as a poroviscoelastic Maxwell material with temperature-dependent Lamé coefficients and viscosities. These parameters crucially depend on a moisture-dependent glass transition temperature, which signals the transition from a predominantly poroelastic material at low temperatures to a poroviscoelastic material at high temperatures. The governing poroviscoelastic equations are then coupled to a multiphase model to determine the temperature, water saturation, and vapour pressure within the bean, and are then used as input variables to determine the radial stress and displacement of a spherically symmetric bean. We find that if the viscosity of the material changes significantly at the glass transition temperature, a large spike of stress occurs, which may signal the onset of macro-scale deformations such as First Crack. Therefore, by controlling when the glass transition temperature occurs at a given location within the bean (say, by modifying the roasting temperature or the convective heat transfer coefficient at the bean's surface), one may control when First Crack occurs in a particular roast.

Our results suggest a fairly simple caricature for the processes leading to First Crack. Thermal diffusion is relatively large, and hence the temperature within the bean is fairly uniform. However, water diffusion is much slower, and thus the outer shell of the bean dries more quickly than the interior. This results in a non-uniform glass transition temperature throughout the bean. In particular, most of the interior of the bean, which has higher water content, passes through the glass transition first and becomes mechanically weak. Meanwhile, an outer shell is formed on the surface of the bean, which remains below the glass transition temperature. This outer shell remains mechanically strong, and results in a build up of internal stress. Eventually, the increased stress becomes large enough for failure to occur near the surface, possibly through brittle fracture (not analysed here). Note that this mechanism is different from the idea of fracture due to high gas pressures in an entirely elastic bean.

While we have a mechanical understanding of the processes leading up to First Crack, there are many aspects of coffee bean roasting that have not been considered in this work. Many parameter values in the models, such as the Lamé coefficients and viscosities of solid coffee beans, are unknown and further experimental work may refine these parameter values. One significant assumption we have used throughout is that the bean can be modelled as a spherically symmetric structure, in order ot generate simple results. However, considering more accurate and realistic geometries would prove useful in understanding specific features of the spatially heterogeneous fracture mechanics at First Crack. Finally, the model we consider describes the roasting of an isolated coffee bean, and future work will consider multi-bean configurations more representative of industrial scale roasting.

Acknowledgments

This publication is based on work supported by the EPSRC Centre for Doctoral Training in Industrially Focused Mathematical Modelling (EP/L015803/1) in collaboration with Jacobs Douwe Egberts (JDE). N. Fadai thanks JDE for financial support and the opportunity to work on-site during parts of this project. The authors thank R. Farr (JDE) for helpful discussions.

[1] J. Baggenstoss. *Coffee roasting and quenching technology - Formation and stability of aroma compounds*. PhD thesis, Swiss Federal Institute of Technology, 2008.

[2] V. Chandrasekar and R. Viswanathan. Physical and thermal properties of coffee. *Journal of Agricultural Engineering Research*, 73(3):227–234, 1999.

[3] J. A. Dean. *Lange's Handbook of Chemistry, 15th Ed.* McGraw-Hill, New York, 1999.

[4] G. Eggleston, B. J. Trask-Morrell, and J. R. Vercellotti. Use of differential scanning calorimetry and thermogravimetric analysis to characterize the thermal degradation of crystalline sucrose and dried sucrose-salt residues. *Journal of Agricultural and Food Chemistry*, 44(10):3319–3325, 1996.

[5] A. Fabbri, C. Cevoli, L. Alessandrini, and S. Romani. Numerical modeling of heat and mass transfer during coffee roasting process. *Journal of Food Engineering*, 105(2):264–269, 2011.

[6] N. T. Fadai, Z. Akram, F. Guilmineau, J. Melrose, C. P. Please, and R. A. Van Gorder. The influence of distributed chemical reaction groups in a multiphase coffee bean roasting model. *IMA Journal of Applied Mathematics*, 83:821–848, 2018.

[7] N. T. Fadai, J. Melrose, C. P. Please, A. Schulman, and R. A. Van Gorder. A heat and mass transfer study of coffee bean roasting. *International Journal of Heat and Mass Transfer*, 104:787–799, 2017.

[8] N. T. Fadai, C. P. Please, and R. A. Van Gorder. Asymptotic analysis of a multiphase drying model motivated by coffee bean roasting. *SIAM Journal on Applied Mathematics*, 78(1):418–436, 2018.

[9] G. J. Fan, H. Choo, and P. K. Liaw. A new criterion for the glass-forming ability of liquids. *Journal of Non-Crystalline Solids*, 353(1):102–107, 2007.

[10] S. E. Fayle and J. A. Gerrard. *The Maillard Reaction*, volume 5. Royal Society of Chemistry, 2002.

[11] M. Fukuhara, M. Yagi, and A. Matsuo. Temperature dependence of elastic parameters and internal frictions for tini alloy. *Physical Review B*, 65(22):224210, 2002.

[12] L. J. Gibson and M. F. Ashby. *Cellular solids: structure and properties*. Cambridge University Press, 1999.

[13] A. N. Gloess, A. Vietri, F. Wieland, S. Smrke, B. Schönbächler, J. A. Sánchez López, S. Petrozzi, S. Bongers, T. Koziorowski, and C. Yeretzian. Evidence of different flavour formation dynamics by roasting coffee from different origins: On-line analysis with ptr-tof-ms. *International Journal of Mass Spectrometry*, 365:324–337, 2014.

[14] S. Gökmen. Effects of moisture content and popping method on popping characteristics of popcorn. *Journal of Food Engineering*, 65(3):357–362, 2004.

[15] F. E. Heuze. High-temperature mechanical, physical and thermal properties of granitic rock - a review. In *International Journal of Rock Mechanics and Mining Sciences & Geomechanics Abstracts*, volume 20, pages 3–10. Elsevier, 1983.

[16] P. Howell, G. Kozyreff, and J. Ockendon. *Applied Solid Mechanics*, volume 43. Cambridge University Press, 2009.

[17] M. Kaseem, K. Hamad, J. H. Park, and Y. G. Ko. Rheological properties of abs/wood composites. *European Journal of Wood and Wood Products*, 73(5):701–703, 2015.

[18] I. Langmuir. The vapor pressure of metallic tungsten. *Physical Review*, 2(5):329, 1913.

[19] S. I. F. S. Martins, W. M. F. Jongen, and M. A. J. S. Van Boekel. A review of maillard reaction in food and implications to kinetic modelling. *Trends in Food Science & Technology*, 11(9-10):364–373, 2000.

[20] L. Oltean, A. Teischinger, and C. Hansmann. Influence of temperature on cracking and mechanical properties of wood during wood drying–a review. *BioResources*, 2(4):789–811, 2007.

[21] C. R. Oswin. The kinetics of package life. iii. the isotherm. *Journal of Chemical Technology and Biotechnology*, 65(12):419–421, 1946.

[22] R. Perren, R. Geiger, S. Schenker, and F. Scher. Recent developments in coffee roasting technology. In *20th International Conference on Coffee Science*, pages 451–459. Association for science and information on coffee, 2004.

[23] R. J. Poole. The deborah and weissenberg numbers. *British Society of Rheology, Rheology Bulletin*, 53:32–39, 2012.

[24] L. Roberts, E. Nordgård-Hansen, Ø. Mikkelsen, S. A. Halvorsen, and R. A. Van Gorder. A heat and mass transfer study of carbon paste baking. *International Communications in Heat and Mass Transfer*, 88:9–19, 2017.

[25] N. L. Salmen and G. L. Back. The influence of water on the glass transition temperature of cellulose. *Tappi*, 60(12):137–140, 1977.

[26] S. Schenker. *Investigations on the hot air roasting of coffee*. PhD thesis, Swiss Federal Institute of Technology, 2000.

[27] J. M. Talbot. *Grounds for agreement: The political economy of the coffee commodity chain*. Rowman & Littlefield Publishers, 2004.

[28] R. Uzuoka and R. I. Borja. Dynamics of unsaturated poroelastic solids at finite strain. *International Journal for Numerical and Analytical Methods in Geomechanics*, 36(13):1535–1573, 2012.

[29] M. Z. Zhu, Y. F. Chen, W. B. Zhu, X. M. Du, J. B. Zhou, C. Gu, and R. J. Liao. Mechanical property of hydrous amorphous cellulose studied by molecular dynamics. *Russian Journal of Physical Chemistry B*, 10(3):524–530, 2016.